

RNA-Sequencing Reveals Oligodendrocyte and Neuronal Transcripts in Microglia Relevant to Central Nervous System Disease

Anne C. Solga,¹ Winnie W. Pong,¹ Jason Walker,² Todd Wylie,² Vincent Magrini,² Anthony J. Apicelli,¹ Malachi Griffith,² Obi L. Griffith,² Shinichi Kohsaka,³ Gregory F. Wu,¹ David L. Brody,¹ Elaine R. Mardis,² and David H. Gutmann¹

Expression profiling of distinct central nervous system (CNS) cell populations has been employed to facilitate disease classification and to provide insights into the molecular basis of brain pathology. One important cell type implicated in a wide variety of CNS disease states is the resident brain macrophage (microglia). In these studies, microglia are often isolated from dissociated brain tissue by flow sorting procedures [fluorescence-activated cell sorting (FACS)] or from postnatal glial cultures by mechanic isolation. Given the highly dynamic and state-dependent functions of these cells, the use of FACS or short-term culture methods may not accurately capture the biology of brain microglia. In the current study, we performed RNA-sequencing using *Cx3cr1^{+/GFP}* labeled microglia isolated from the brainstem of 6-week-old mice to compare the transcriptomes of FACS-sorted versus laser capture microdissection (LCM). While both isolation techniques resulted in a large number of shared (common) transcripts, we identified transcripts unique to FACS-isolated and LCM-captured microglia. In particular, ~50% of these LCM-isolated microglial transcripts represented genes typically associated with neurons and glia. While these transcripts clearly localized to microglia using complementary methods, they were not translated into protein. Following the induction of murine experimental autoimmune encephalomyelitis, increased oligodendrocyte and neuronal transcripts were detected in microglia, while only the myelin basic protein oligodendrocyte transcript was increased in microglia after traumatic brain injury. Collectively, these findings have implications for the design and interpretation of microglia transcriptome-based investigations.

GLIA 2014;00:000–000

Key words: laser-capture microdissection, fluorescence-activated cell sorting, macrophage

Introduction

Advances in RNA-sequencing methodologies now enable researchers to study the individual contributions of select cell types to disease (Ozsolak and Milos, 2011). In the setting of central nervous system (CNS) pathology, microglia both respond to and participate in neurological disease. Microglia resemble immune system-like cells (macrophages) that origi-

nate either from the bone marrow during postnatal life (monocytes) or mature within the developing brain during embryogenesis (microglia). As such, microglia have been implicated in the pathogenesis of numerous disorders affecting the CNS, including brain tumors (Graeber et al., 2002; Roggendorf et al., 1996), multiple sclerosis (Jack et al., 2005; Matsumoto et al., 1992), amyotrophic lateral sclerosis (Lewis

View this article online at wileyonlinelibrary.com. DOI: 10.1002/glia.22754

Published online Month 00, 2014 in Wiley Online Library (wileyonlinelibrary.com). Received Mar 12, 2014, Accepted for publication Sep 9, 2014.

Address correspondence to David H. Gutmann, Department of Neurology, Box 8111, 660 South Euclid Avenue, St. Louis, MO 63110, USA.
E-mail: gutmann@neuro.wustl.edu

From the ¹Department of Neurology, Washington University School of Medicine, St. Louis, Missouri; ²The Genome Institute, Washington University School of Medicine, St. Louis, Missouri; ³Department of Neurochemistry, National Institute of Neuroscience, Kodaira, Tokyo, Japan.

WWP, VM, ERM, and DHG jointly supervised research. WWP, ACS, ERM, and DHG conceived and designed the experiments. JW, TW, VM, GFW, and DLB contributed to experimental design. WWP, ACS, and AJA performed the experiments. WWP, ACS, JW, TW, VM, MG, and OLG analyzed the data. VM, GFW, SK, ERM, DLB, and DHG contributed reagents/materials/analysis tools. WWP, ACS, JW, TW, VM, MG, and OLG contributed to the preparation of the manuscript. WWP, ACS, and DHG wrote the article. All authors edited and approved the article.

Anne C. Solga and Winnie W. Pong contributed equally to this work.

Additional Supporting Information may be found in the online version of this article.

et al., 2012), Alzheimer's disease (Davis et al., 1992; Meda et al., 1995; Sasaki et al., 1997), and traumatic brain injury (TBI; Hernandez-Ontiveros et al., 2013; Ramlackhansingh et al., 2011). Their seminal roles in initiating and promoting CNS disease have resulted in early phase clinical studies that target microglia function using non-selective inhibitors (e.g., minocycline). Unfortunately, these trials failed to demonstrate efficacy (Casha et al., 2012), highlighting the need to target the specific products elaborated by these stromal cell types.

The development of therapeutic strategies that target microglia-produced factors requires the identification of microglia transcripts in both health and in the context of neurological disease. Several methods are now typically employed for these studies, including microglia culture *in vitro* (Hassan et al., 1991; Ohtaki et al., 2013; Szabo and Gulya, 2013), fluorescence-activated cell sorting (FACS; Hassan et al., 1991), laser capture microdissection (LCM; Waller et al., 2012), and ribosome messenger RNA (mRNA)-trap (BacTRAP and Ribo-Tag) technologies (Heiman et al., 2008; Sanz et al., 2009). While each of these approaches has its strengths and limitations, there are two major barriers to these discovery efforts: First, the RNA routinely isolated from microglia is in low abundance and frequently of low quality, necessitating new methods for RNA isolation and analysis (Pong et al., 2013b; Tariq et al., 2011).

Second, microglia are highly dynamic cells (Parkhurst and Gan, 2010), which change their morphology and expression profile in response to their local environment. In this regard, *in vitro* adaptation results in microglia activation and expression of transcripts not found *in vivo* (Hurley et al., 1999). Moreover, these activated microglia produce an enhanced inflammatory response which is toxic to neurons, and likely does not accurately recapitulate their natural state in the brain (Dheen et al., 2007; Kaindl et al., 2012; Kettenmann et al., 2013). For this reason, it is important to study microglia *in situ*. Since microglia-specific Ribo-TRAP mice are not currently available, there has been a heavy reliance on LCM- or FACS-based methodologies.

In the current report, we sought to leverage optimized RNA-sequencing methods to compare the transcriptomes obtained from LCM- versus FACS-isolated *Cx3cr1*^{+ /GFP} microglia. While both isolation techniques revealed a majority of shared transcripts, we were able to identify transcripts unique to either FACS- or LCM-isolated microglia. Of the LCM-specific microglial transcripts, the majority represented genes typically associated with neurons or glia. While these transcripts were shown to localize to microglia, they were not translated into protein. Moreover, in the setting of two experimental mouse models of CNS pathology, neuronal and oligodendroglial transcripts were increased in microglia following the induction of experimental autoimmune encephalo-

myelitis (EAE), whereas the myelin basic protein oligodendrocyte transcript was increased after TBI.

Materials and Methods

Mice

Wild-type (WT; C57Bl/6), *Cx3cr1*^{+ /GFP} (Jung et al., 2000), and Iba1-EGFP (Hirasawa et al., 2005) mice were maintained on a C57Bl/6 background and used in accordance with approved Animal Study Committee protocols at the Washington University School of Medicine. Mice were euthanized at 6 weeks of age, and tissues were collected for histological analyses, RNA expression, LCM, and FACS.

EAE was induced by injecting myelin oligodendrocyte glycoprotein (MOG) peptide fragment 35–55 (MEVGWYRSPFSRVVHLYRNGK; CS Bio Company, Menlo Park, CA) dissolved in complete Freund's adjuvant (CFA) into Iba1-EGFP mice ($n = 4$), followed by two injections of 200 ng Pertussis toxin (Enzo Life Sciences, Farmingdale, NY). Neurological functional tests were performed using a five-point standardized rating scale: 0 = no clinical signs; 1 = tail paralysis; 2 = mild hind limb weakness; 3 = moderate to severe hind limb paresis; 4 = complete hind limb paralysis and partial forelimb weakness; and 5 = moribund state or death (Racke, 2001). Animals were collected post-immunization days 10–14 at clinical score 2. Control animals ($n = 4$) received CFA-only injections.

Controlled cortical impact (CCI) experimental TBI was induced in 8-week-old Iba1-EGFP mice ($n = 4$). Following induction of anesthesia with isoflurane (5% induction, 2% maintenance) and positioning on a stereotaxic frame, a 5.0-mm left lateral craniotomy was performed. The CCI injury was produced by impacting a 3.0-mm diameter metal tip onto the cortex (5 m/s, 100 ms dwell time) centered at 2.7 mm lateral to midline and 3.0 mm anterior to lambda with an impact depth of 2.0 mm. This produces a moderately severe contusion in the left sensorimotor cortex and underlying hippocampus. The sham group consisted of mice that received a craniotomy, but not a cortical impact ($n = 4$). Following the injury, a plastic skull cap was secured over the craniotomy, and the skin incision was sutured. Mice were kept at 37°C throughout the procedure and during recovery until return of normal ambulation (Tran et al., 2011). Animals were euthanized at 7 days following the experimental injury, when numbers of microglia were observed to be the highest (Jiang and Brody, 2012).

Isolation of Microglial Cells for FACS

Pools of 6–10 mouse brainstems per experiment were collected, triturated and passed through a prewetted 70 μ m cell strainer. Enzymatic dissociation was performed by incubation of tissue with collagenase and DNase I (Sigma, St. Louis, MO) for 1 h at room temperature while gently rocking. The digested brain tissue was then passed through a 40- μ m cell strainer and collected by centrifugation at 300g for 10 min at 4°C.

For microglia enrichment, cells were applied to a Percoll density-gradient. Percoll solutions with different densities have been used. To yield a stock isotonic Percoll solution (90%, density 1.123 g/mL), nine volume parts of Percoll (density 1.13 g/mL;

Sigma) were mixed with one volume part of 1.5 M NaCl (density 1.058 g/mL). Percoll solutions with various percentages [70% (1.1 g/mL), 37% (1.05 g/mL), and 30% (1.04 g/mL)] were prepared via dilution of 90% Percoll with 1× phosphate buffered saline (PBS) or Hank's balanced salt solution with phenol red. The gradient was then centrifuged for 30 min at 1,200g without braking.

For FACS, the cell layer at the 70%/37% interface was collected, washed with PBS (containing 1% fetal bovine serum and 0.1% sodium azide) to dilute the contaminating Percoll, followed by centrifugation for 10 min at 300g. Microglia were then processed for antibody-mediated flow sorting (Supp. Info. Table 1) using appropriate controls for gating, as previously described (Simmons et al., 2011). Brainstem microglia from WT mice were CD11b⁺ CD45^{low} and microglia from *Cx3cr1*^{+/-GFP} mice were CD11b⁺ CD45^{low} GFP⁺. FACS samples were sorted directly into TRIzol (Life Technologies Corporation, Carlsbad, CA) for total RNA extraction (Supp. Info. Table 2). Sorting was performed at the High-Speed Cell Sorter Core Facility at the Siteman Cancer Center, Washington University, and data were subsequently analyzed using FlowJo (Tree Star, Ashland, OR).

For RNA fluorescence in situ hybridization (RNA FISH) analysis, both interfaces (70%/37% and 37%/30%) were collected.

Laser-Capture Microdissection

Brainstems dissected from anesthetized and Ringer's solution-perfused *Cx3cr1*^{+/-GFP} mice were sectioned into 1 mm thick sections on ice and placed immediately into cold 4% paraformaldehyde in PBS containing ProtectRNATM RNase Inhibitor (Sigma, St. Louis, MO) for 5 minutes. Sections were washed, embedded in Tissue-Tek O.C.T. Compound (Tissue-Tek, Miles, Elkhart, IN), cryosectioned at 7 μm thickness, and mounted on PEN-membrane slides for collection on a LMD7000 system (Leica Microsystems, Wetzlar, Germany). A total oval area of 170–175 μm² was collected for each GFP⁺ cell and approximately 1,000 cells per sample were collected for RNA extraction in lysis buffer [10 mM Tris-HCl (pH 7.9), 50 mM EDTA (pH 7.9), 0.2 M NaCl, 2.2% SDS, 1,000 μg/mL proteinase K, 2 U/μL RNaseOUT; Invitrogen, Grand Island, NY; Supp. Info. Table 2].

RNA Isolation

TRIzol-chloroform extraction was used to isolate total RNA from flow sorted cell pellets. Extracted RNA samples were resuspended in Ambion Nuclease-free water (Life Technologies Corporation), snap frozen, and stored at -80°C. An optimized proteinase K/acid phenol protocol was used to extract RNA from LCM samples (Khodosevich et al., 2007). Briefly, cells collected in lysis buffer were incubated at 55°C overnight, and the RNA was isolated in 1:1 phenol (pH 4.2) and chloroform. Total RNA was resuspended in Ambion Nuclease-free water (Life Technologies Corporation), and treated with DNase prior to storage at -80°C and quality assessment.

RNA was treated with TURBO DNA-free kit (Invitrogen) to eliminate residual DNA prior to quality and yield analysis using the Agilent Eukaryotic Total RNA 6000. RNA quantification was

performed using the Quant-iTTM RNA assay kit on a QubitTM Fluorometer (Life Technologies Corporation).

RNA-Seq

The Ovation[®] RNA-Seq method was employed for complementary DNA (cDNA) synthesis according to the manufacturer's instructions (NuGen, San Carlos, CA). cDNA was then concentrated and suspended in 10 mM Tris-HCl (pH 7.6) using the MinElute spin column (Qiagen, Valencia, CA), followed by assessment of the concentration, using the Quant-iTTM dsDNA HS Assay (Life Technologies Corporation), and the molecular weight distribution, using the BioAnalyzer 2100 and the Agilent DNA 7500 Chip Assay (Agilent Technologies, Santa Clara, CA).

500 ng cDNA (10 ng/μL) was used for Illumina library construction with the Illumina paired-end LT indexing protocol as previously published (Govindan et al., 2012; Mardis et al., 2009). For each library ligation, polymerase chain reaction (PCR) optimization was performed to prevent over-amplification. For LCM-isolated samples, 120218_LCM_F, 120324_LCM_M, 120414_LCM_F, and 120530_LCM_M (Supp. Info. Table 2), the PCR optimization procedure used 1 μL of ligated sample into the KAPA SYBRFAST Universal 2× quantitative PCR (qPCR) Master Mix protocol (Kapa Biosystems, Woburn, MA) and the universal Illumina library primers P5 (5' AATGATACGGCGACCACCGAGATCTA) and P7 (5' CAAGCAGAAGACGGCATACGAGAT), and samples were amplified using the Eppendorf epigradient S qPCR instrument (98° × 2 min, 30 cycles of 98° × 10 s, and 65°C × 30 s). The optimal PCR cycle for each sample was determined based on the inflection point of the Ct curve and was assessed as 11 cycles for all samples.

The FACS-isolated samples, 1135739, 1135740, 1135741, 1135742, 1135743, and 1135744 (Supp. Info. Table 2), were processed prior to qPCR-based cycle optimizations. Thus, 1 μL of each ligated product was amplified using 2× Phusion High-Fidelity PCR Master Mix with HF Buffer (New England BioLabs, Ipswich, MA) and 200 nM P5 and P7 primers and cycled as follows: 98° × 2 min, 20 cycles of 98° × 10 s, 65°C × 30 s, and 72°C × 30 s, with a final hold at 72°C. 5 μL aliquots were removed from the reactions at cycle numbers 8, 10, 12, 14, 16, and 18. Each aliquot was qualitatively assessed for both amplification product and size using the 2.2% FlashGelTM System (Lonza Group, Basel, Switzerland). The optimal cycle number was determined based on the presence of amplified library with minimal overcycled by-products. For each library, the optimal cycle numbers were between 13 and 18.

For all library amplifications, nine PCR reactions per sample were performed using the 2× Phusion High-Fidelity PCR Master Mix as described above and cycled as follows: 98° × 2 min, "N" cycles of 98° × 10 s, 65°C × 30 s, and 72°C × 30 s with a final hold at 72°C; where "N" is the optimal cycle number, which had been determined in the prior amplification reaction. Each PCR-amplified library was combined and purified using MinElute PCR Purification columns according to manufacturer's protocol (Qiagen). Each amplified ligation was then assessed for concentration using Quant-iTTM dsDNA HS Assay (Life Technologies Corporation) and for size using the BioAnalyzer 2100 and the Agilent DNA 1000 Assay (Agilent Technologies).

500 ng of each library from FACS- or LCM-isolated samples were used for SureSelectXT Mouse All Exon capture (Agilent Technologies). This reagent targets 221,784 exons (49.6 Mb) based on the NCBI37/mm9 Mouse genome assembly. Capture libraries were subsequently sized to ~300–500 bp using a 1:0.6 sample to AMPureXP bead ratio to which the supernatants were added to 0.9× volumes of beads. The resulting supernatants were discarded, the beads washed, and size-fractionated capture libraries were eluted and diluted to 2 nM stocks for subsequent Illumina sequencing. Corresponding RNA-Seq paired end reads were processed using the TopHat (Trapnell et al., 2009) and Cufflinks suite (Trapnell et al., 2010; Roberts et al., 2011a, b). Fragments per kilobase per million mapped reads (FPKM) values for each transcript and gene were used to generate transcript levels for comparisons between the different sample types: FACS_WT (wild-type microglia isolated by FACS), FACS_GFP (*Cx3cr1*^{+GFP} microglia isolated by FACS), and LCM_GFP (*Cx3cr1*^{+GFP} microglia isolated by LCM). Due to FPKM values of zero that can naturally result from Exome capture experiments, calculations were facilitated by adding a value of 1 to all FPKM (FPKM + 1) prior to fold change calculations and log₂ transformation (FC).

Immunofluorescence

Following anesthetization, mice were transcardially perfused with Ringer's solution and 4% paraformaldehyde in phosphate buffer. Dissected tissues were postfixed overnight and processed for O.C.T. Compound embedding. Immunofluorescence was performed using appropriate antibodies (Supp. Info. Table 1) and Tyramide Signal Amplification kits (Life Technologies Corporation), followed by DAPI counterstaining. Images of the medulla region of the brainstem (Supp. Info. Fig. 1) were subsequently acquired on a Nikon Eclipse TE300 fluorescence inverted microscope (Nikon, Tokyo, Japan) equipped with an optical camera (Optronics, Goleta, CA) and MetaMorph image analysis software (Molecular Devices, Downton, PA).

RNA Fluorescence In Situ Hybridization

FISH was performed using QuantiGene ViewRNA kit (Affymetrix, Frederick, MD) according to the manufacturer's instructions with minor modifications. The conditions were optimized to include a 10-min protease treatment. The oligonucleotide probes were commercially designed using the murine *Mbp* (Accession number NM_001025245.1), *Mobp* (NM_001039364.2), *Mag* (NM_010758.2), *Syn2* (NM_001111015.1), *Crmp1* (NM_001136058.2), and *Nmnat2* (NM_175460.3) sequences. Representative images of the medulla region of the brainstem (Supp. Info. Fig. 1) were obtained on a Nikon Eclipse TE300 fluorescence inverted microscope (Nikon) and analyzed using MetaMorph image analysis software (Molecular Devices). Individual mRNA punctae in the GFP-positive cells were manually counted, and mRNA molecules per GFP⁺ microglia and total cells were calculated. All analyses were performed in a blinded fashion.

To verify the localization of the mRNA molecules, representative z-stack images were obtained using a confocal microscope (Olympus FV-500) in green (argon laser) and red (krypton laser) channels and subsequently z-projected.

Statistical Analysis

Statistical analysis was performed using GraphPad Prism 5.0 software (GraphPad, La Jolla, CA). Data are represented as mean values ± standard error of the mean (SEM). Statistical significance (set at $P < 0.05$) was assessed by using the Student's two-tailed *t*-test. The Grubbs' outlier test was used to determine statistical outliers.

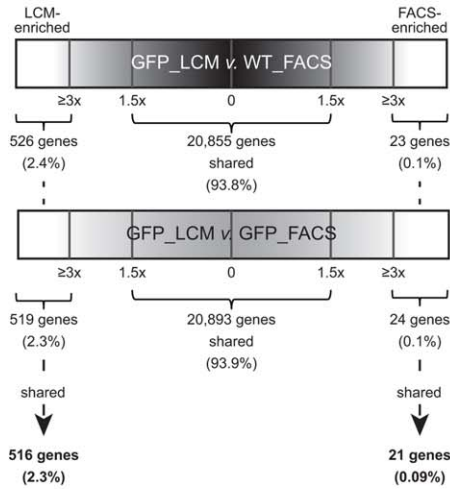
Results

To compare the RNA expression profiles of microglial cells obtained by FACS and LCM, microglia were isolated from wild-type (CD11b⁺ CD45^{low}) and *Cx3cr1*^{+GFP} (CD11b⁺ CD45^{low} GFP⁺) brainstems using FACS (Supp. Info. Fig. 2A) or LCM, based on GFP expression (Supp. Info. Fig. 2B). Histological sections obtained from brain tissue of *Cx3cr1*^{+GFP} transgenic mice confirmed specific GFP expression in Iba1-expressing cells (microglia; Supp. Info. Fig. 2C). To generate an accurate transcriptome from extremely limited material (e.g., LCM-isolated samples), combined exome capture enrichment and Illumina RNA-sequencing (cDNA-Capture sequencing) was performed on all samples (Supp. Info. Table 2).

Samples were analyzed using the Cufflinks platform (Roberts et al., 2011a, b; Trapnell et al., 2010) to calculate differential expression of genes from each sample. Fewer than 0.5% of the genes detected differed between wild-type (WT_FACS) and *Cx3cr1*^{+GFP} microglia isolated by FACS (GFP_FACS; Supp. Info. Fig. 2D), while a greater number of genes differed between microglia of either genotype collected by FACS relative to those collected by LCM (Fig. 1A). Because we were unable to accurately and rapidly detect wild-type microglia lacking GFP expression by LCM, we utilized a combination of differential gene expression methods to identify transcripts uniquely expressed in LCM-collected microglia, regardless of genotype. First, *Cx3cr1*^{+GFP} microglia isolated by LCM (GFP_LCM) were compared with WT_FACS, resulting in 526 transcripts enriched in GFP_LCM (2.4%). Similarly, microglia transcripts from GFP_LCM compared with GFP_FACS resulted in 519 transcripts enriched in GFP_LCM (2.3%). The intersection of these two transcript lists allowed us to identify 516 transcripts shared between LCM-collected microglia, independent of the *Cx3cr1* genotype (Fig. 1A and Supp. Info. Table 3). The intersection of transcripts that are highly expressed in FACS-isolated microglia resulted in 21 transcripts (0.09%; Fig. 1A and Supp. Info. Table 4).

We next prioritized transcripts by filtering the lists such that there was a difference in expression of at least FPKM > 1 between the FACS-isolated and LCM-isolated samples, resulting in 1,047 transcripts with greater expression in LCM-collected microglia (Supp. Info. Table 3) and 125 transcripts with higher expression in FACS-sorted microglia (Supp. Info. Table 4). We then focused on transcripts expressed at a range

A



B

transcript	name	GFP_FACS > GFP_LCM (FC)	WT_FACS > GFP_LCM (FC)
<i>Hist1h1d</i>	histone cluster 1, H1d	6.17	5.97
<i>Hist1h3d</i>	histone cluster 1, H3d	5.73	5.73
<i>Hist1h1c</i>	histone cluster 1, H1c	5.69	5.63
<i>Junb</i>	Jun-B oncogene	5.29	5.60
<i>Otud1</i>	OTU domain containing 1	5.01	5.07
<i>Jun</i>	Jun oncogene	5.00	5.35
<i>Adamts1</i>	a disintegrin-like and metalloproteinase (reprolysin type) with thrombospondin type 1 motif, 1	4.43	4.66
<i>Olf1029</i>	olfactory receptor 1029	4.42	3.81
<i>Blg2</i>	B cell translocation gene 2, anti-proliferative	4.15	4.48
<i>Imp2l</i>	IMP2 inner mitochondrial membrane peptidase-like (S. cerevisiae)	4.06	3.85
<i>Cxcl10</i>	chemokine (C-X-C motif) ligand 10	4.02	4.28
<i>Gm17576</i>	predicted gene, 17576	3.98	3.35
<i>Egr1</i>	early growth response 1	3.95	3.93
<i>Zfp36</i>	zinc finger protein 36	3.80	3.82
<i>Abcb1b</i>	ATP-binding cassette, subfamily B (MDR/TAP), member 1B	3.41	3.51
<i>Neur3</i>	neuronal homolog 3 homolog (Drosophila)	3.38	3.63
<i>Abca1</i>	ATP-binding cassette, subfamily A (ABC1), member 1	3.37	3.47
<i>Hist2h3c1</i>	histone cluster 2, H3c1	3.23	3.35
<i>Tagap</i>	T cell activation Rho GTPase activating protein	3.22	3.54
<i>Slamf1</i>	signaling lymphocytic activation molecule family member 1	3.11	3.15
<i>Leprel1</i>	leprecan-like 1	3.03	3.18

C

	transcript	name	GFP_LCM > GFP_FACS (FC)	GFP_LCM > WT_FACS (FC)
oligodendroglial transcripts	<i>Mbp</i>	Myelin basic protein	8.78	8.73
	<i>Mobp</i>	Myelin-associated oligodendrocytic basic protein	7.85	7.62
	<i>Mag</i>	Myelin-associated glycoprotein	3.20	3.16
neuronal transcripts	<i>Syn2</i>	Synapsin II	3.64	3.64
	<i>Crmp1</i>	Collapsin response mediator protein 1	3.42	3.35
	<i>Nmnat2</i>	Nicotinamide nucleotide adenylyltransferase 2	3.07	3.07

of ≥ 3 -fold change for further RNA validation as well as protein expression by immunofluorescence.

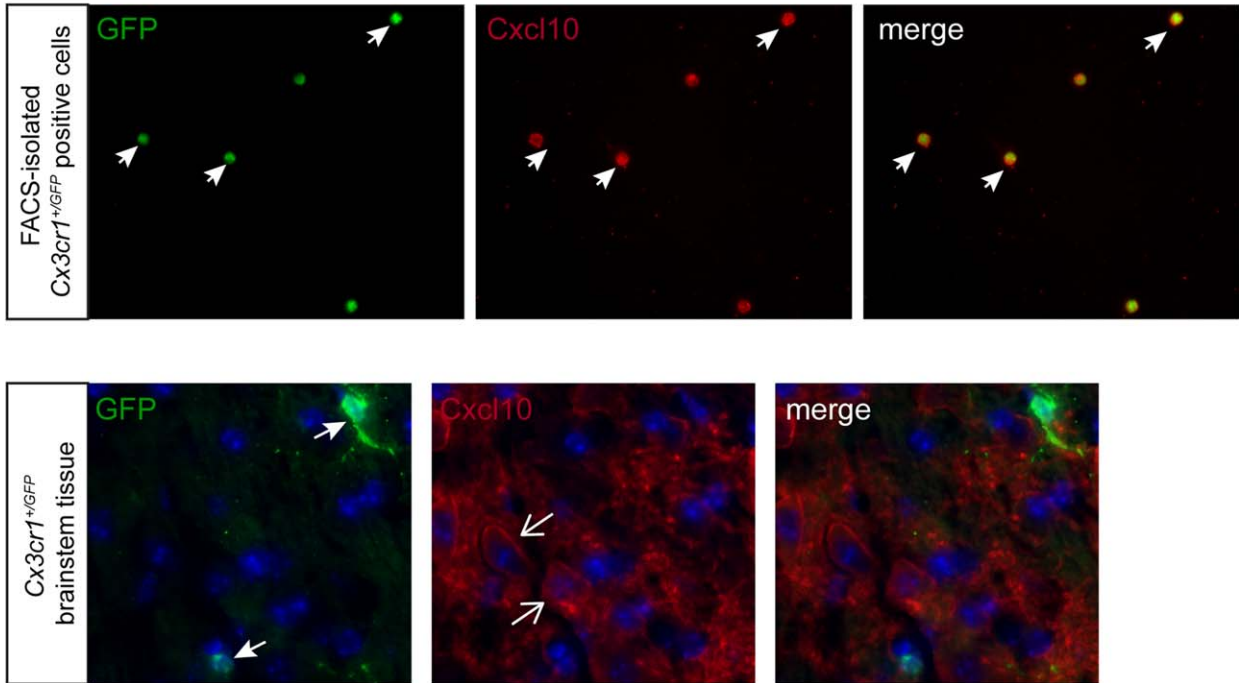
Analysis of the transcripts enriched in FACS-isolated microglia showed high expression of genes implicated in transcriptional control, including four genes belonging to the histone cluster family important for chromatin structure (e.g., *Hist1h1d*, *Hist1h3d*, *Hist1h1c*, and *Hist2h3c1*; Izzo et al., 2008) and three involved in the regulation of transcription (e.g., *Jun-B*, *Jun* and *Egr1*; Petersohn and Thiel, 1996; Windak et al., 2013). Other transcripts included those relevant to lymphocyte function (e.g., *Slamf1*, *Tagap*; Veillette et al., 2007), cholesterol transport (e.g., *Abcb1b*, *Abca1*; Oram and Vaughan, 2000), and inflammatory processes (e.g., *Cxcl10*, *Adamts1*; Klein, 2004; Lemarchant et al., 2013; Fig. 1B). To validate the differential expression of a subset of these transcripts, we performed immunostaining of FACS-sorted GFP⁺ microglial cells or *Cx3cr1*^{+/GFP} brainstem sections using commercially available Cxcl10 and c-Jun antibodies, and confirmed the protein expression of these transcripts in FACS-isolated microglia, but not in normal brain microglia *in situ* (Fig. 2).

Conversely, LCM-isolated microglia expressed transcripts typically found in neurons and glia (Fig. 1C and Supp. Info. Table 5). The majority of transcripts discovered were neuron-specific (e.g., *Crmp1*, *Syn2*, *Nmnat2*; Cahoy et al., 2008; Doyle et al., 2008; Wang and Strittmatter, 1996) or involved in oligodendrocyte function (e.g., *Mbp*, *Mobp*, *Mag*; Cahoy et al., 2008; Doyle et al., 2008; Fig. 1C). This cell type specificity was confirmed by immunohistochemistry on normal brain, demonstrating Mobp protein expression in APC-labeled oligodendrocytes and Nmnat2 protein expression in NeuN-labeled neurons (Supp. Info. Fig. 3).

To determine whether the neuron or oligodendrocyte-specific transcripts were localized and expressed in *Cx3cr1*^{+/GFP} microglia, we performed RNA FISH and

FIGURE 1: Selection of transcripts for validation. (A) Schematic representation of the transcripts shared and differentially expressed in LCM- and FACS-isolated microglia. The black bar denotes comparisons between WT microglia isolated by FACS (WT_FACS) and *Cx3cr1*^{+/GFP} microglia isolated by LCM (GFP_LCM), while the gray bar denotes *Cx3cr1*^{+/GFP} microglia isolated by FACS (GFP_FACS) and *Cx3cr1*^{+/GFP} microglia isolated by LCM (GFP_LCM). ~94% of the transcripts were shared between microglia isolated by FACS and LCM. Transcripts with a ≥ 3 fold change (FC) were classified as enriched for LCM-isolated (516 transcripts; 2.3%) or FACS-isolated (21 transcripts; 0.09%) microglia. Candidate transcripts were selected for validation based on a range of FC, importance in microglia function, and cell-type specificity. **(B)** Transcripts in FACS-sorted microglia show enrichment of transcripts that are involved in several different biological processes, whereas **(C)** transcripts in LCM-collected microglia are associated with the enrichment of transcripts that are linked to neurons and oligodendrocytes.

A



B

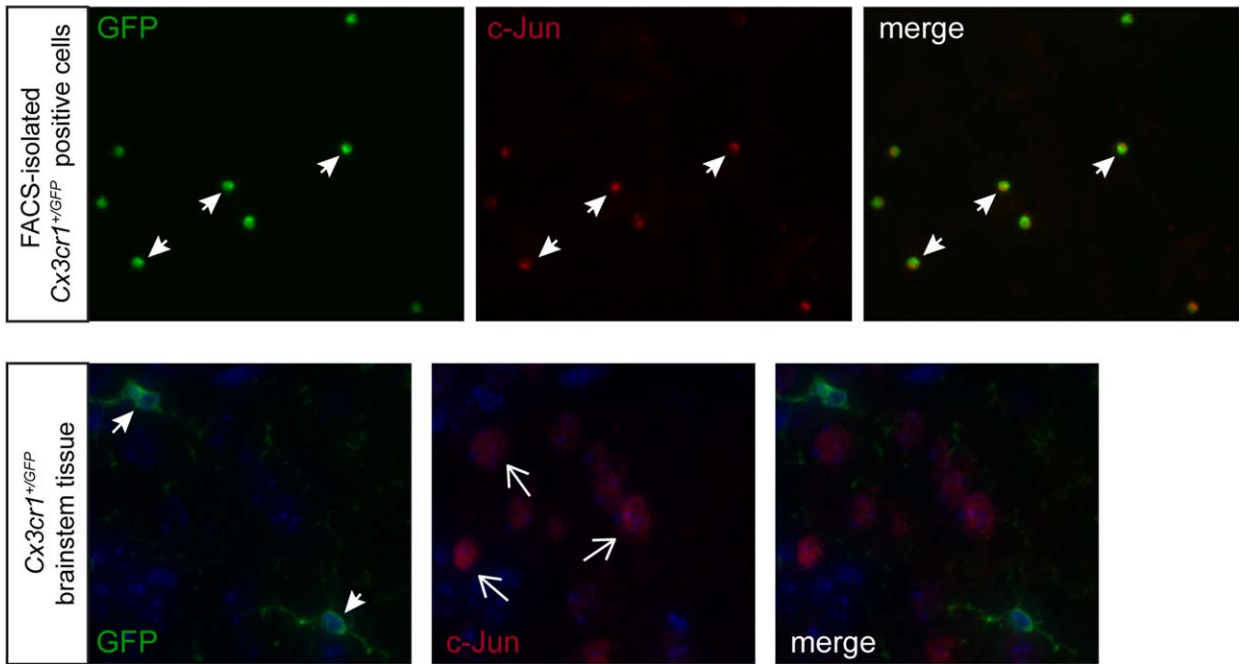


FIGURE 2: FACS-enriched transcripts are not expressed in GFP⁺ microglia *in situ*. Immunofluorescence analysis of FACS-sorted Cx3cr1^{+/GFP} microglia and Cx3cr1^{+/GFP} tissue cryosections using Cxcl10 (A) and c-Jun (B) antibodies shows that FACS-sorted GFP-positive microglia express these proteins, whereas GFP-positive microglia in Cx3cr1^{+/GFP} tissue sections do not express these proteins. The nuclei were counterstained with DAPI (blue). Representative images are shown.

immunohistochemistry, respectively. RNA FISH revealed RNA punctae within cell bodies in 28–91% of GFP⁺ microglia, depending on the transcript (Figs. 3 and 4). This was confirmed using high resolution *z*-stack confocal microscopy (Fig. 3C). In contrast, *Mobp* and *Nmnat2* protein expression was not detected in GFP⁺ microglia *in situ* (Figs. 3D and 4C).

Based on previous experiments in our laboratory and others suggesting that impaired *Cx3cr1* expression in *Cx3cr1*^{+GFP} mice has consequences for microglia function in the retina (Liang et al., 2009) and is associated with low-grade brain tumors (Pong et al., 2013a), we next employed Iba1-EGFP mice (Hirasawa et al., 2005) as a complementary microglia-specific reporter strain for transcript validation by RNA FISH. Similar to the results obtained using *Cx3cr1*^{+GFP} mice, 27–87% of Iba1-EGFP microglia also contained mRNA punctae (Figs. 4 and 5). In addition, we also performed experiments to demonstrate that these oligodendrocytic and neuronal transcripts were also localized to microglia from other regions of the CNS: as observed in the brainstem, these transcripts were also found in microglia within the spinal cord and hippocampus of Iba1-EGFP mice (Suppl. Info. Figs. 4 and 5).

To determine at what stage during tissue processing microglial neuron- and oligodendrocyte-specific transcript localization was lost, *Cx3cr1*^{+GFP} cells were subjected to RNA FISH at various times during processing. In these experiments, RNA FISH was performed (1) immediately following the trituration and cell strainer step, (2) after Percoll density gradient centrifugation, and (3) at the end of FACS isolation (Fig. 6A). mRNA punctae were only detected following tissue homogenization, but not in the 70%/37% interface after Percoll density gradient centrifugation or FACS isolation (Fig. 6B). Since previous studies have suggested that macrophages from different Percoll fractions are functionally heterogeneous (Bielefeldt Ohmann and Babiuk, 1986; O’Neill et al., 1984; Plasman and Vray, 1993; Rasmussen et al., 1983), we additionally isolated and analyzed microglia from the 37%/30% Percoll interface, and found that these harbored increased mRNA punctae for all transcripts (Fig. 6B).

To determine whether the abundance of these oligodendrocyte- and neuron-specific transcripts was influenced by nervous system disease states characterized by microglial infiltration, we analyzed their expression in two experimental murine neurological disease models (EAE and TBI).

In the setting of EAE, spinal cords of Iba1-EGFP mice were analyzed by RNA FISH at a clinical grade of 2 (Fig. 7A). RNA FISH revealed oligodendroglial (*Mbp* and *Mobp*; Fig. 7B and Supp. Info. Fig. 7) and neuronal (*Crmp1* and *Nmnat2*; Fig. 8A and Supp. Info. Fig. 6) mRNA punctae in GFP⁺ microglia at baseline and in response to EAE. Following MOG induction, more microglia with ≥ 2 mRNA mole-

cules per GFP⁺ cell were observed (Figs. 7C and 8B, left panels). The increase in *Mbp* and *Crmp1* transcripts in MOG-treated mice was specific to microglia and was not seen in the surrounding cells (Figs. 7C and 8B, right and middle panels). Despite a greater abundance of *Mbp* and *Crmp1* transcripts in MOG-treated mice, neither *Mbp* nor *Crmp1* were translated into protein in GFP⁺ microglia, as assessed by antibody-based immunofluorescence (Figs. 7D and 8C).

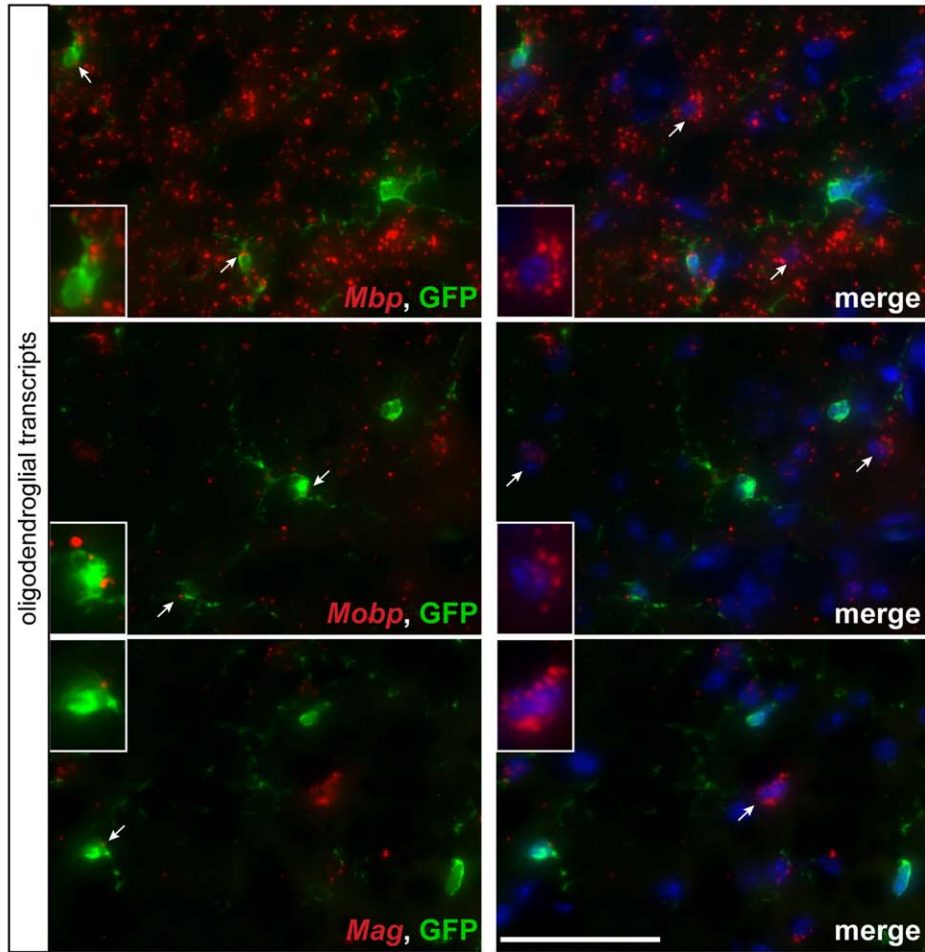
Next, we employed a moderately severe CCI TBI model, which generates contusions in the left sensorimotor cortex and hippocampus. Brains were removed for RNA FISH analysis 7 days postinjury from 8-week-old Iba1-EGFP mice (Fig. 9A). In contrast to the EAE model, RNA FISH revealed only increased *Mbp* transcripts in hippocampal GFP⁺ microglia (Fig. 9B), with injured mice demonstrating ≥ 2 mRNA *Mbp* molecules per GFP⁺ cell relative to control mice (Fig. 9C, left panel). The increase in *Mbp* transcripts in injured mice was only observed in the microglia, and not in the surrounding cells (Fig. 9C, right and middle panel). Similar to EAE, there were no GFP⁺ microglia expressing *Mbp*, using antibody-based immunofluorescence (Figs. 9D and 10).

Discussion

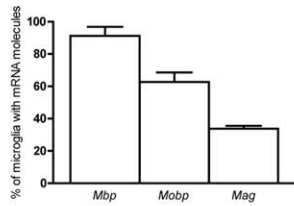
Faithful representation of the *in vivo* global transcriptional state of any given class of neural cells using expression profiling techniques is encumbered by the underlying structure of brain tissue, which is typified by heterogeneous, spatially intermingled cell types, distributed in varying proportions. To study cell type-specific gene expression, it is critical to employ methods that optimize selectivity for one class of cells relative to all others, while minimizing the potential for artificially perturbing transcript expression in the process. To this end, we sought to examine and compare the global transcriptional profiles of microglia isolated either by FACS or LCM. To generate an accurate transcriptome from extremely limited material (e.g., LCM-isolated samples), combined exome capture enrichment and Illumina RNA sequencing (cDNA-Capture sequencing) was performed. The combination of exome capture and RNA-Seq has been shown to offer improved results over conventional RNA-Seq by enriching for coding regions. It is specifically designed to increase the representation of the lowest expressed genes in the transcriptome, while minimizing oversequencing of the most highly expressed genes (Cabanski et al., 2014). The development of this advanced technology herein has revealed several important findings.

First, the vast majority of transcripts (94%) were identified using both methods, suggesting that either technique is useful for global discovery efforts. In this regard, genes previously reported as microglia-expressed transcripts were detected,

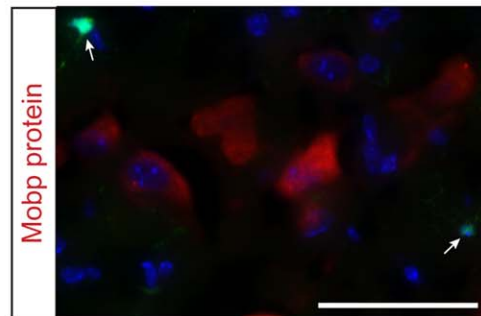
A



B



D



C

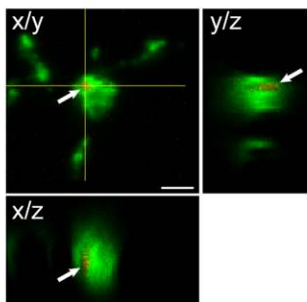


FIGURE 3: Fluorescent *in situ* hybridization confirms the localization of oligodendrocyte-specific transcripts in *Cx3cr1^{+/GFP}* microglia. (A) RNA FISH reveals oligodendrocyte-specific (*Mbp*, *Mobp*, *Mag*) mRNA punctae (red) in 34–91% (B) of GFP⁺ microglia. Representative images are shown with insets of GFP-positive microglia as well as GFP-negative cells containing mRNA molecules. Scale bar, 50 μm. (C) A representative high resolution confocal z-stack projection demonstrates *Mag* mRNA puncta in GFP-positive microglia. Arrow points to the co-localization of mRNA and GFP fluorescence (yellow color). *x/y*, *x/z*, and *y/z* projections are shown to confirm the intracellular localization of mRNA within a microglial cell body. Scale bar, 5 μm. (D) Immunofluorescence analysis of paraformaldehyde-fixed tissue cryosections using *Mobp* antibodies (red) and endogenous GFP (green) shows that the *Mobp* mRNA present in *Cx3cr1^{+/GFP}* microglia is not translated (arrows). The nuclei were counterstained with DAPI (blue). Representative images are shown. Scale bar, 50 μm.

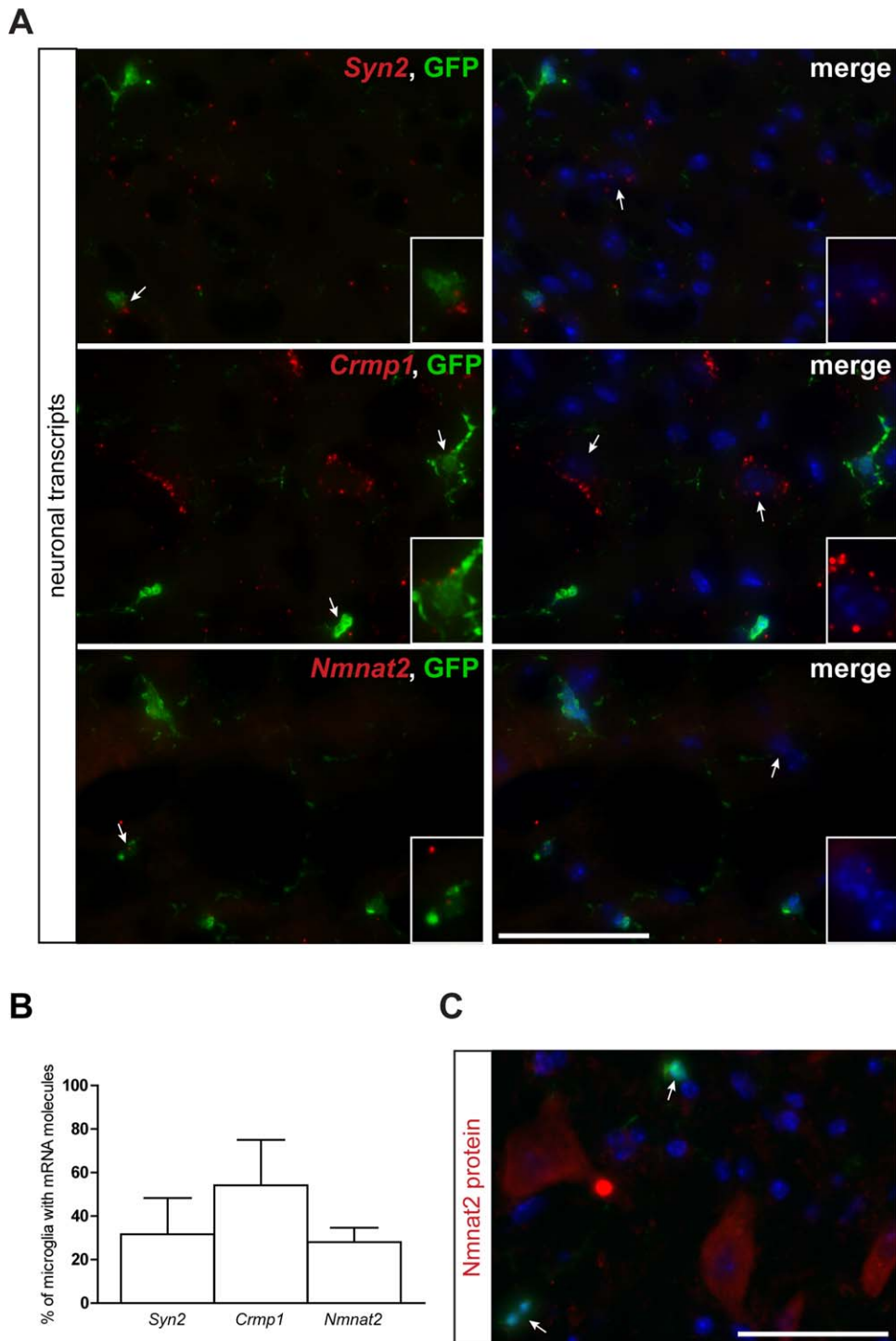


FIGURE 4: Fluorescent *in situ* hybridization confirms the localization of neuron-specific transcripts in *Cx3cr1*^{+/GFP} microglia. (A) RNA FISH reveals neuron-specific (*Syn2*, *Crmp1*, *Nmnat2*) mRNA punctae (red) in 28–54% (B) of GFP⁺ microglia. Representative images are shown with insets of GFP-positive microglia as well as GFP-negative cells containing mRNA molecules. Scale bar, 50 μ m. (C) Immunofluorescence analysis of paraformaldehyde-fixed tissue cryosections using *Nmnat2* antibodies (red) and endogenous GFP (green) shows that the *Nmnat2* mRNA present in *Cx3cr1*^{+/GFP} microglia is not translated (arrows). The nuclei were counterstained with DAPI (blue). Representative images are shown. Scale bar, 50 μ m.

including *Aif1* (Iba1) (Imai et al., 1996), *Cx3cr1* (Boddeke et al., 1999), *CD68* (Penfold et al., 1991), *Emr1* (F4/80; Perry et al., 1985), and *Itgam* (Cd11b; Morimura et al., 1990).

Second, we identified a small number of transcripts enriched in FACS-isolated microglia. These included genes involved in chromatin structure, such as histone cluster

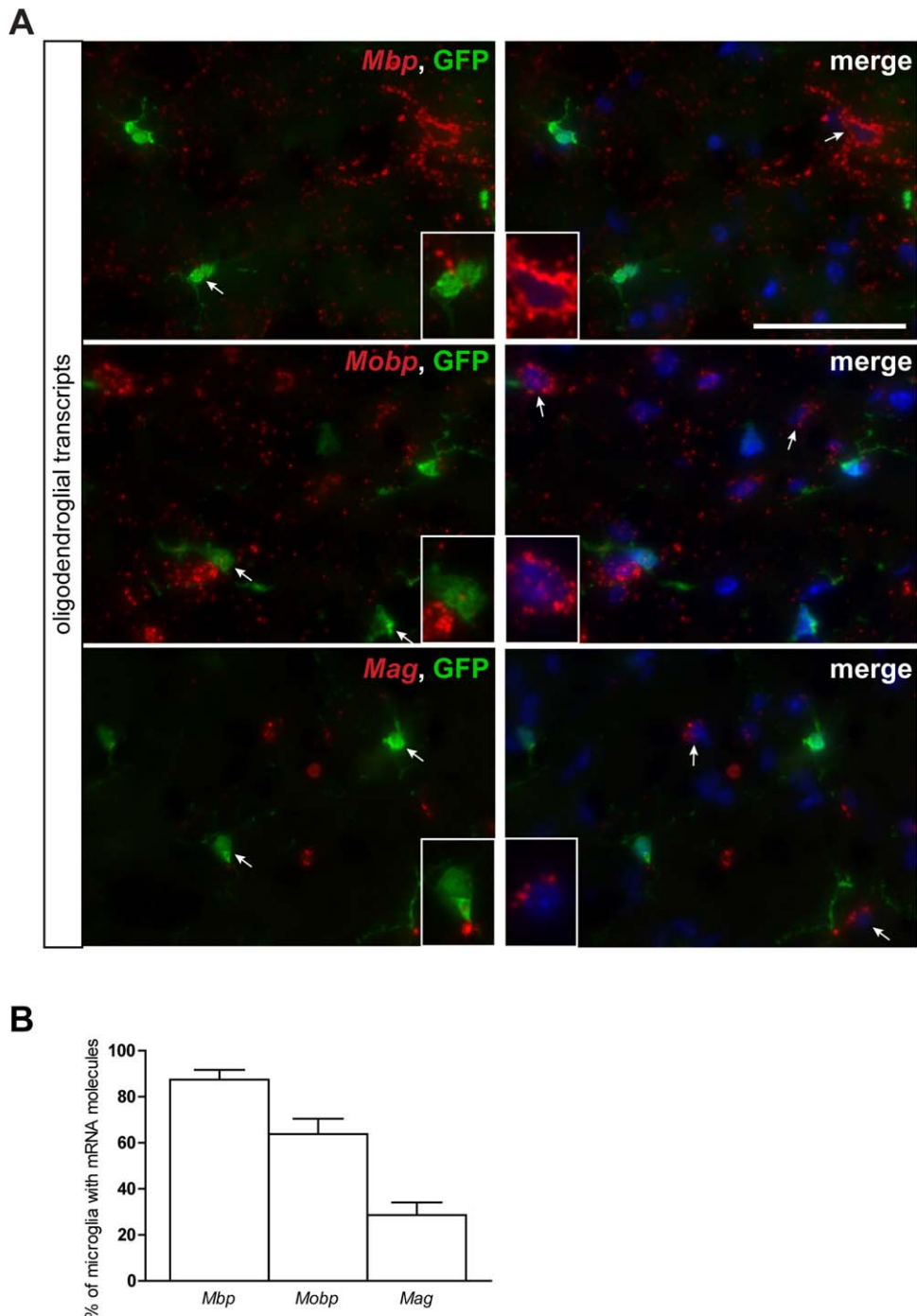


FIGURE 5: Fluorescent *in situ* hybridization confirms the localization of oligodendrocyte-specific transcripts in Iba1-EGFP microglia. (A) RNA FISH reveals oligodendrocyte-specific (*Mbp*, *Mobp*, *Mag*) mRNA punctae (red) in 29–87% (B) of GFP⁺ microglia. The nuclei were counterstained with DAPI (blue). Representative images are shown with insets of GFP-positive microglia as well as GFP-negative cells containing mRNA molecules. Scale bar, 50 μ m.

proteins and transcriptional regulators, like *Egr1*, *Jun*, and *Junb*. In addition, other transcripts were found, encompassing a wide variety of potential functions, ranging from lymphocyte activation (T cell activation GTPase activating protein or CD150) to the CXCL10 chemokine and the ADAM metalloproteinase. While the increased expression of these genes is intriguing, it

would be premature to conclude that they connote a different state of microglia function. Further mechanistic studies will be required to determine whether these FACS-isolated microglia are functionally different than their native counterparts *in situ*.

Third, 50% of the transcripts enriched in LCM-isolated microglia represent genes typically expressed by other differentiated

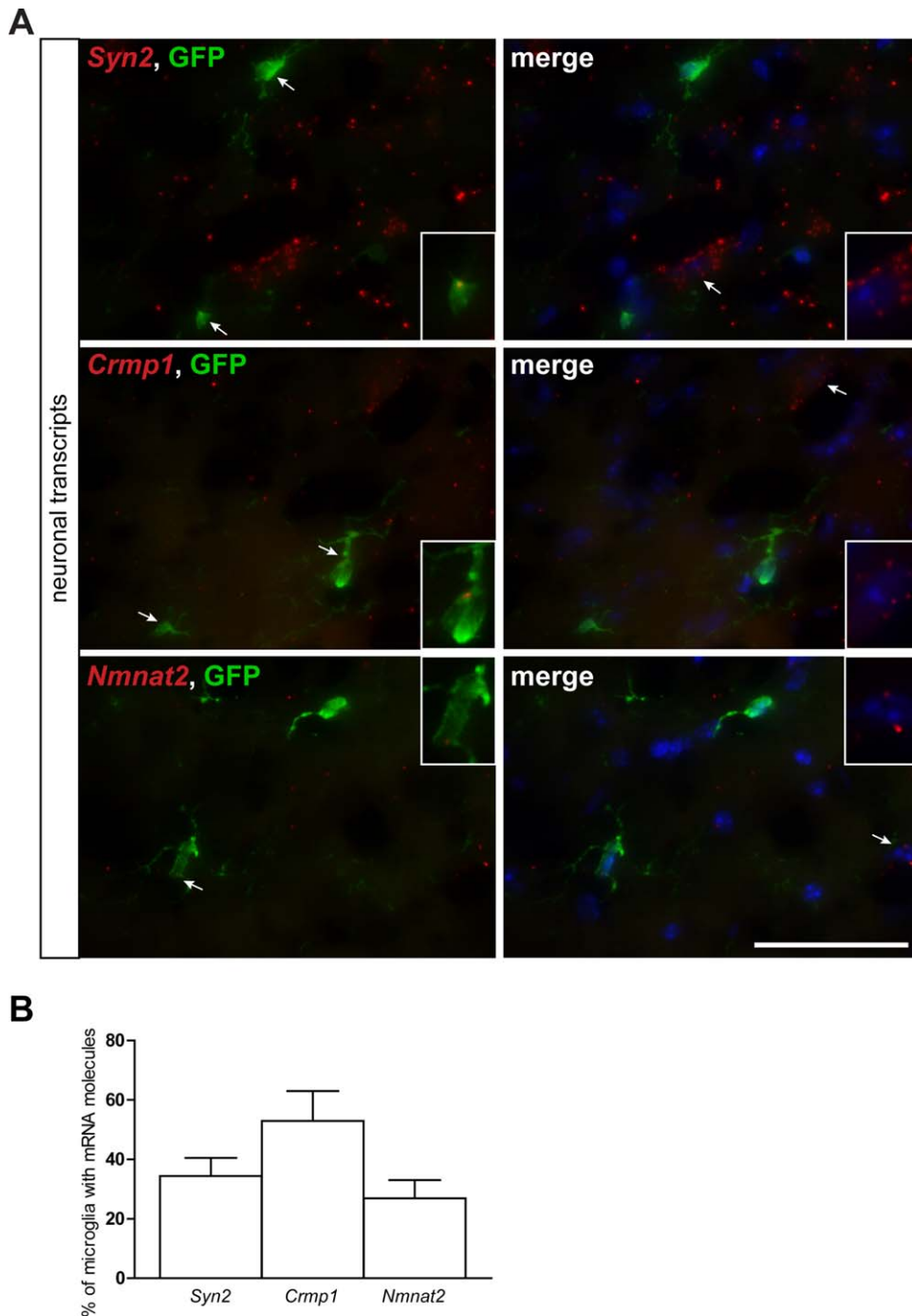


FIGURE 6: Fluorescent *in situ* hybridization confirms the localization of neuron-specific transcripts in Iba1-EGFP microglia. (A) RNA FISH reveals neuron-specific (*Syn2*, *Crmp1*, *Nmnat2*) mRNA punctae (red) in 27–53% (B) of GFP⁺ microglia. The nuclei were counterstained with DAPI (blue). Representative images are shown with insets of GFP-positive microglia as well as GFP-negative cells containing mRNA molecules. Scale bar, 50 μ m.

cell types in the brain. Of these cell type-specific transcripts, the majority were neuronal (60%), with the remainder generally found in oligodendrocytes or astrocytes. Using a combination of complementary methods (RNA-FISH and *z*-stack confocal microscopy), these transcripts were demonstrated to be contained within the microglia themselves. However, within the microglia,

they are not translated into protein. While their role in microglia physiology is not clear, it is possible that their location in microglia reflects phagocytosis of RNA from cells in their local surround. Support for this hypothesis derives from the Percoll gradient experiments, in which RNA-FISH punctae were found in microglia at the 37%/30% interface, where the majority of phagocytic

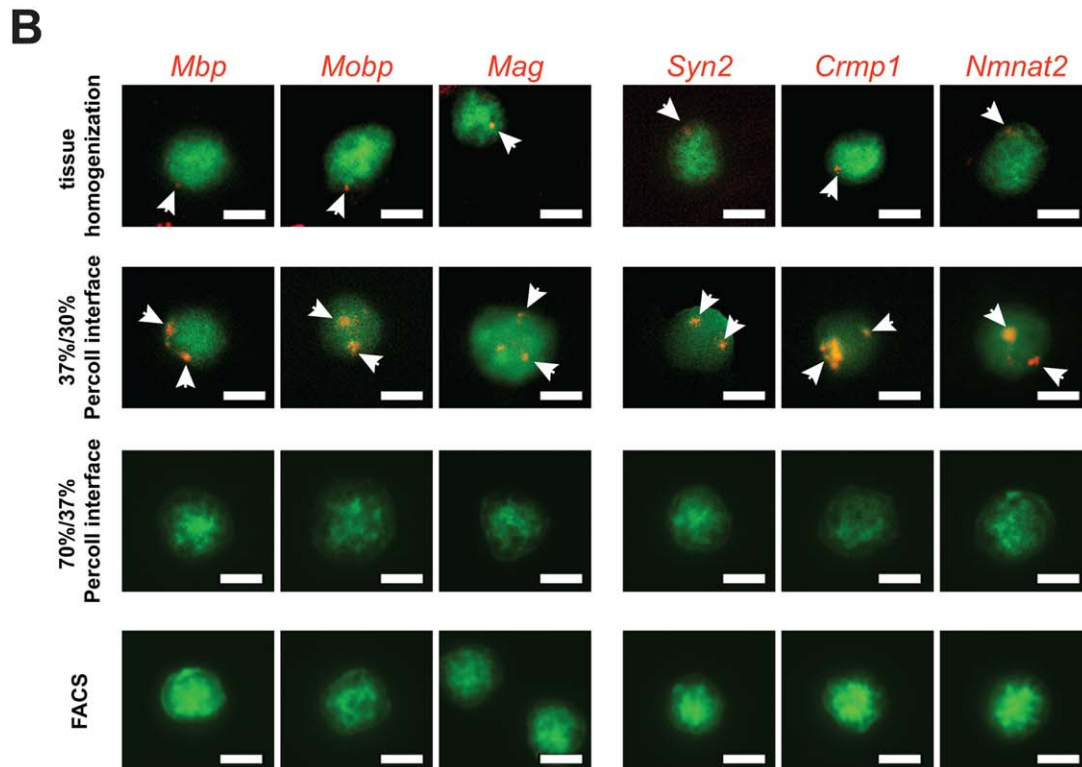
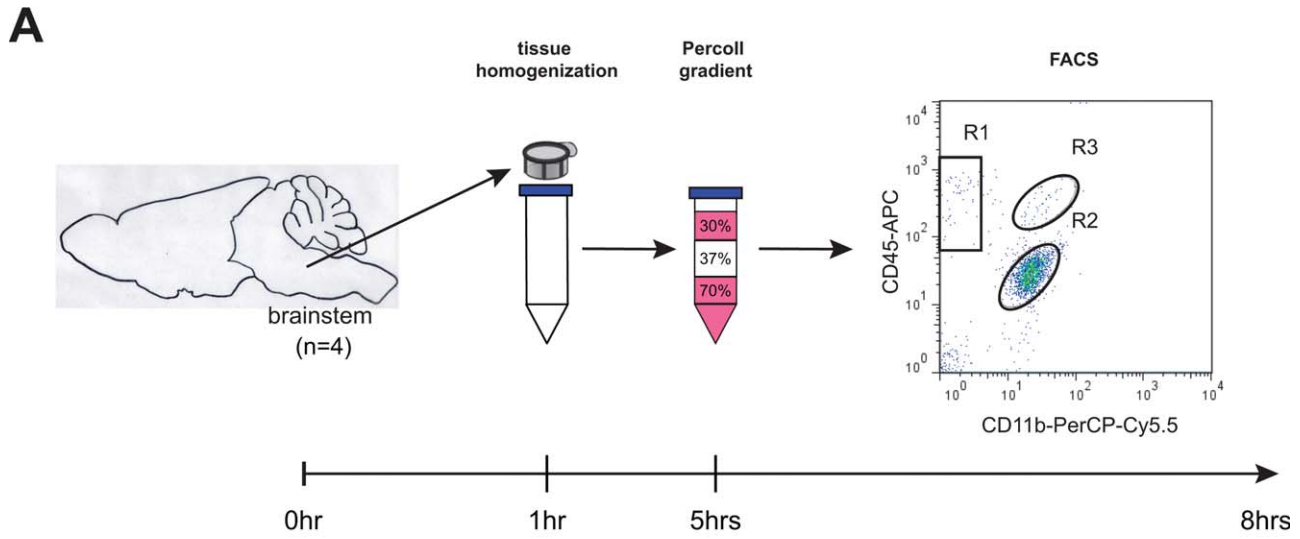


FIGURE 7: RNA FISH analysis of $Cx3cr1^{+/GFP}$ microglia during FACS isolation. (A) Sequence and timing of the steps used in the preparation of GFP^{+} microglia. Microglia were analyzed after (1) the brainstems were triturated and passed through a cell strainer, (2) Percoll density gradient centrifugation, and (3) FACS isolation. **(B)** Following each step, isolated cells were subjected to RNA FISH. Microglia show mRNA punctae (arrow; yellow) only at the beginning of the FACS process (following tissue homogenization), and in the 37%/30% Percoll interface, but not in the 37%/70% Percoll interface or after FACS isolation. Representative images are shown. Scale bar, 5 μ m.

cells are typically located (Chandler et al., 1986). As such, microglia have been reported to engulf exosomes through macropinocytosis, a process similar to phagocytosis, but occurring without evidence of microglial activation (Fitzner et al., 2011). These exosomes have been shown to contain nucleic acids, including mRNAs (Miranda et al., 2014). In this manner, macropinocytosis

clearance could be an important mechanism by which microglia participate in the degradation of mRNA both during normal brain homeostasis and in the setting of CNS pathology. Additional mechanistic studies beyond the scope of this study will be necessary to conclusively demonstrate that microglia mRNA transcript uptake occurs through this process.

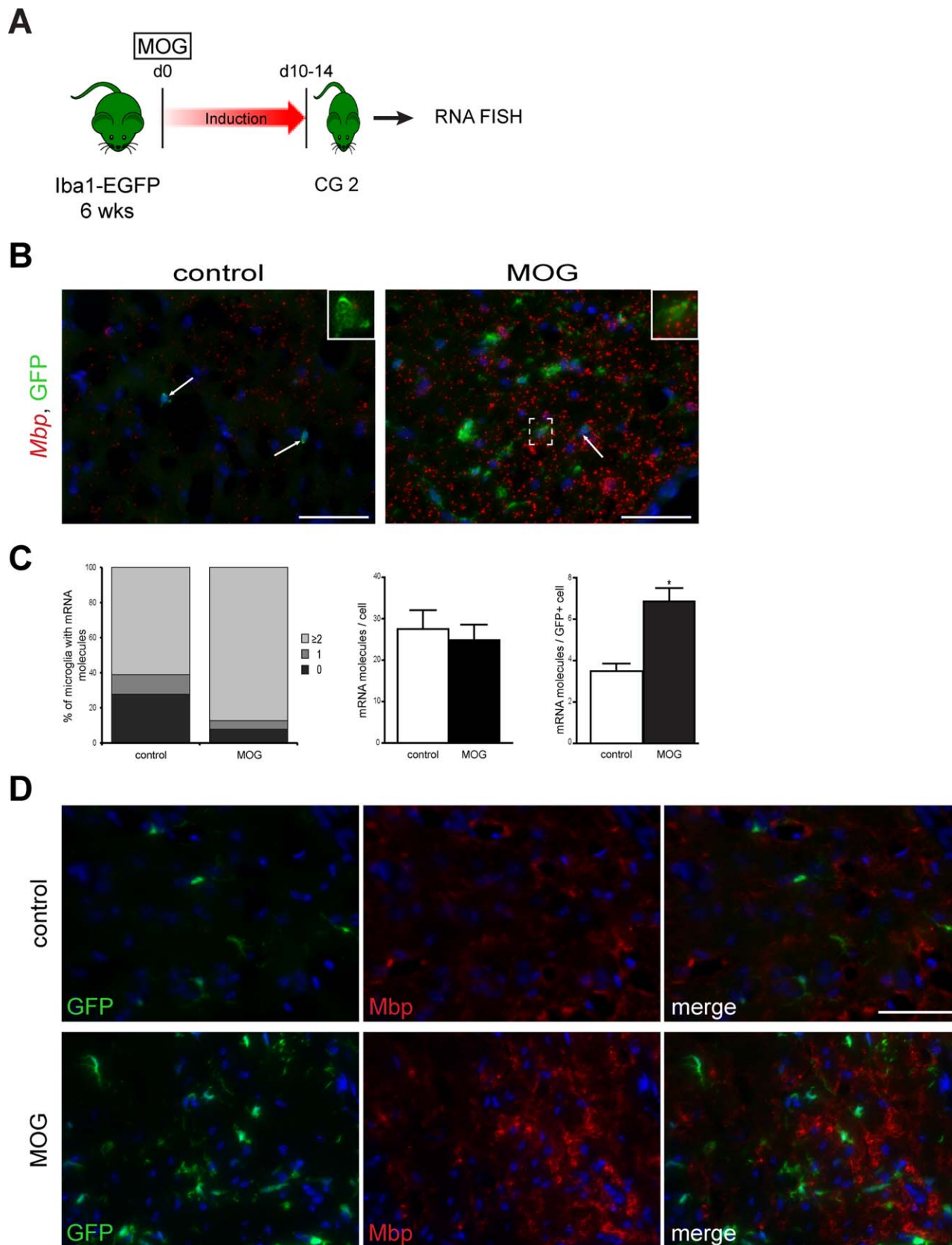


FIGURE 8: Fluorescent *in situ* hybridization shows increased *Mbp* transcript expression after EAE induction. (A) Following EAE induction, mice were euthanized 10–14 days post-injection (clinical grade (CG) 2) for RNA FISH. (B) Fluorescent images of RNA-FISH reveal *Mbp* mRNA punctae (red) in GFP⁺ microglia (green). Representative images are shown with insets of microglia with RNA transcript expression. (C) MOG treatment results in more microglia with ≥ 2 mRNA molecules per GFP⁺ cell relative to control mice (left panels). The increase in *Mbp* transcripts in MOG-treated mice is microglia-specific (right panels) and was not seen in the surrounding cells (middle panels). Each error bar represents the mean \pm SEM. Asterisks denote statistically significant differences (*) $P < 0.0306$. (D) Despite a greater abundance of *Mbp* transcripts in MOG-treated mice, *Mbp* is not translated into protein in GFP⁺ microglia as assessed by antibody-based immunofluorescence. The nuclei were counterstained with DAPI (blue). Scale bar, 50 μ m.

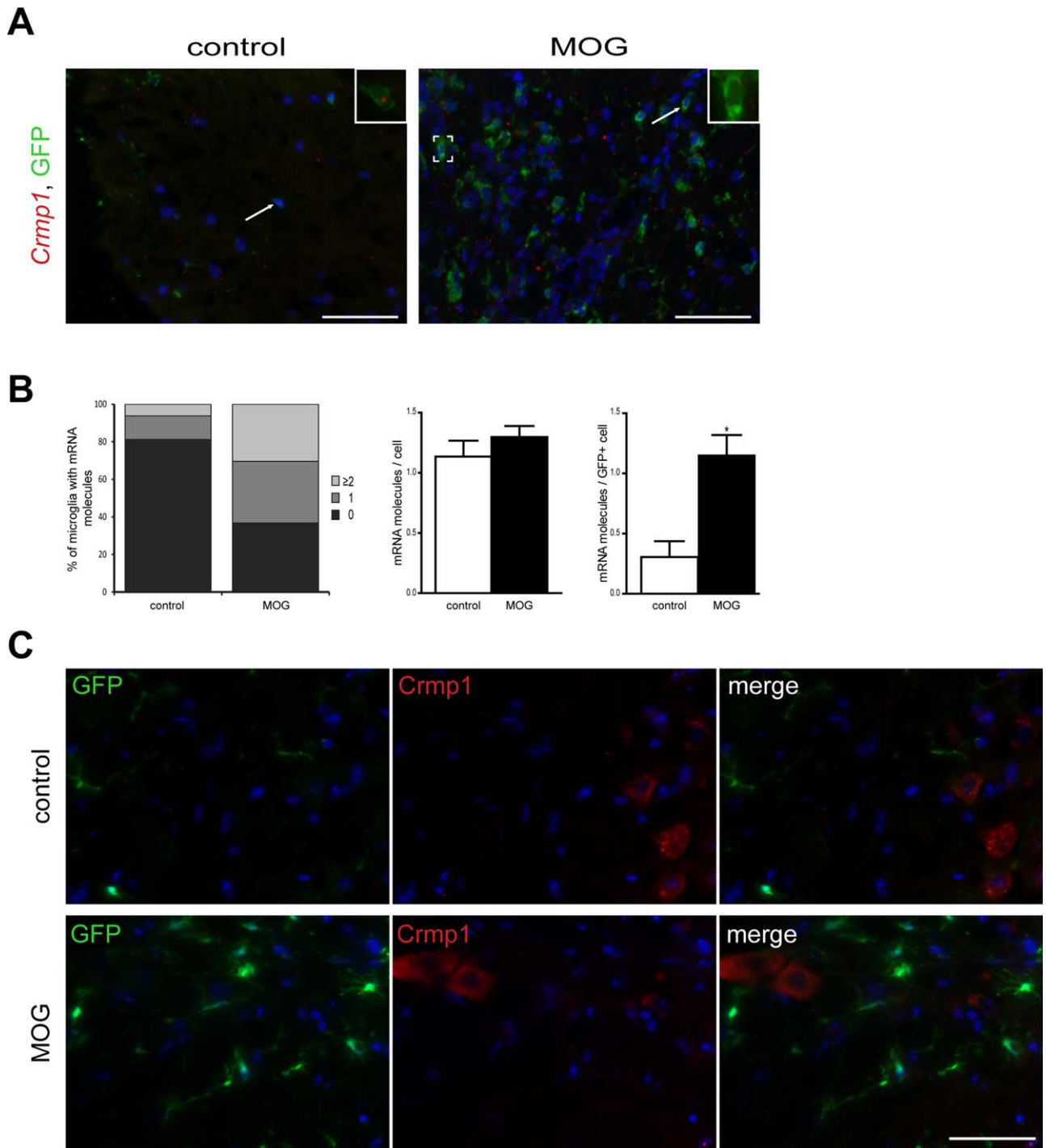


FIGURE 9: Fluorescent *in situ* hybridization shows increased *Crmp1* transcript expression after EAE induction. (A) Fluorescent images of RNA-FISH reveal *Crmp1* mRNA punctae (red) in GFP⁺ microglia (green). Representative images are shown with insets of microglia with RNA transcript expression. (B) MOG treatment results in more microglia with ≥2 mRNA molecules per GFP⁺ cell relative to control mice (left panels). The increase in *Crmp1* transcripts in MOG-treated mice is microglia-specific (right panels) and was not seen in the surrounding cells (middle panels). Each error bar represents the mean ± SEM. Asterisks denote statistically significant differences (*) $P < 0.0306$. (C) Despite a greater abundance of *Crmp1* transcripts in MOG-treated mice, *Crmp1* is not translated into protein in GFP⁺ microglia as assessed by antibody-based immunofluorescence. The nuclei were counterstained with DAPI (blue). Scale bar, 50 μm.

Fourth, we showed that some of these oligodendrocyte and neuron mRNA transcripts are increased in microglia in the setting of two murine models of CNS pathology, EAE

and TBI, which are both characterized by destruction of myelin sheets and axonal loss. The finding that these transcripts are increased in EAE and TBI is also consistent with a

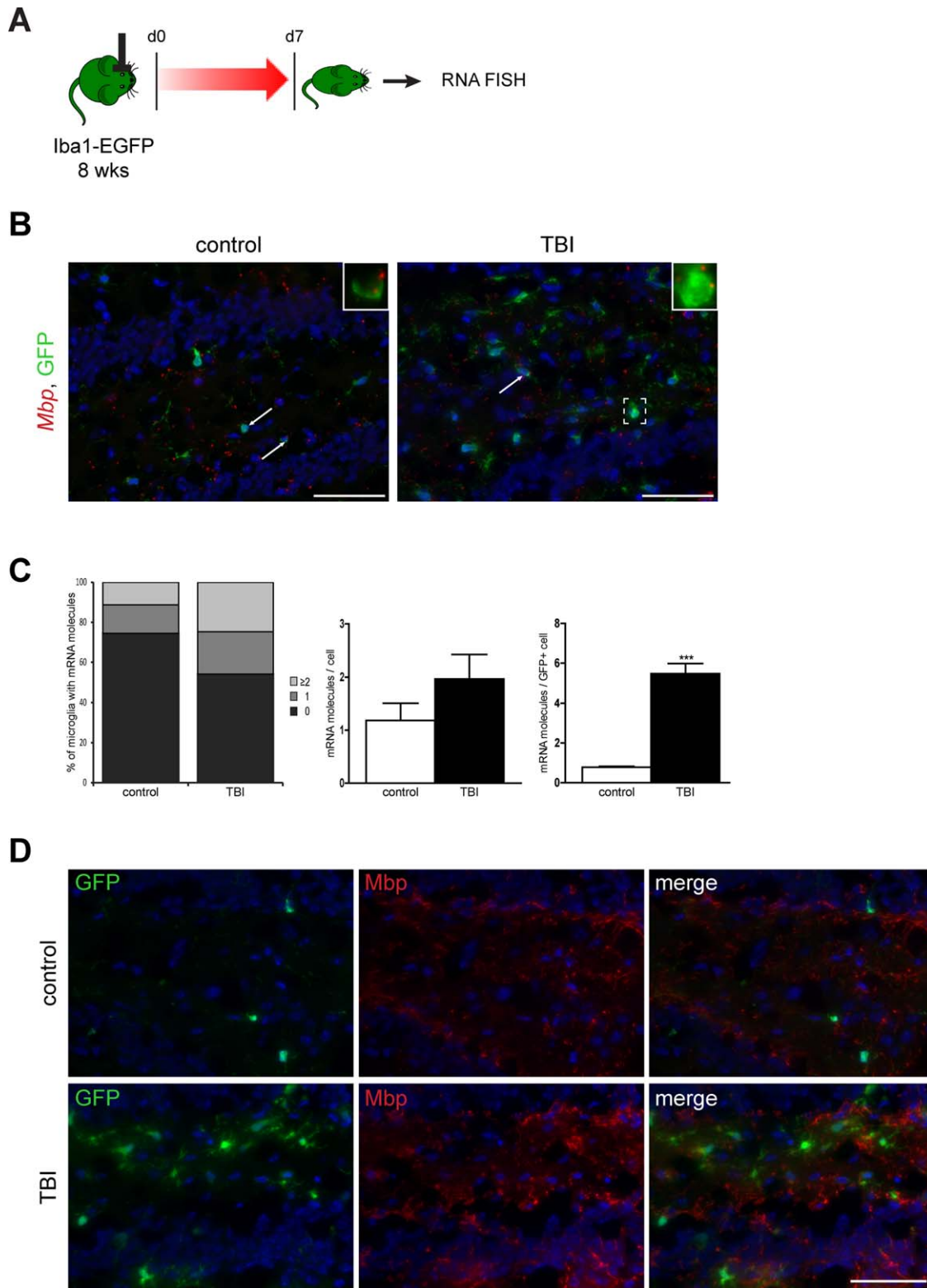


FIGURE 10: Fluorescent *in situ* hybridization shows increased microglia transcript expression after TBI. (A) Following CCI induction, mice were euthanized 7 days post-injury for RNA FISH. (B) Fluorescent images of RNA-FISH reveal *Mbp* mRNA punctae (red) in ipsilateral hippocampal GFP⁺ microglia (green). Representative images are shown with insets of microglia with RNA transcript expression. (C) TBI results in more microglia with ≥ 2 mRNA molecules per GFP⁺ cell relative to control mice (left panel). The increase in *Mbp* transcripts in injured mice is microglia-specific (right panel) and was not seen in the surrounding cells (middle panel). Each error bar represents the mean \pm SEM. Asterisks denote statistically significant differences (***) $P = 0.0001$. (D) Despite a greater abundance of *Mbp* transcripts in hippocampal microglia of injured mice, *Mbp* is not translated into protein in GFP⁺ microglia as assessed by antibody-based immunofluorescence. The nuclei were counterstained with DAPI (blue). Scale bar, 50 μ m.

phagocytic process (Davalos et al., 2012; Gitik et al., 2011; Rinner et al., 1995; Venkatesan et al., 2010), but does not prove that this is the mechanism underlying the enrichment of these neuronal or oligodendroglial transcripts within microglia. Further investigation will be required to define the causative reason for the acquisition of these transcripts in microglia both in health and following CNS injury.

In summary, these findings underscore the importance of appreciating the impact of different isolation methods on microglia transcriptomal analyses. Current and future studies that focus on dynamic and potentially phagocytic cell types isolated from primary tissue should be optimized to provide an accurate representation of the resulting transcriptomes. Future work using BacTrap mice (L10a:EGFP; Heiman et al., 2008), instead of GFP as a reporter, could be employed to enable the capture of transcripts directly from microglia with shorter processing times. The use of this strategy and others should enable the isolation of RNA species associated with ribosomes, potentially facilitating the identification of transcripts actively being translated at the time the tissue is analyzed. Such Iba1 transgenic strains are currently under development.

Acknowledgment

Grant sponsor: NCI Cancer Center Support Grant (to The Siteman Cancer Center); Grant number: #P30 CA91842; Grant sponsor: National Institutes of Health; Grant number: RC4 NS072916 (to DHG); Grant sponsor: W.M. Keck Foundation (to WWP).

We thank the Alvin J. Siteman Cancer Center at Washington University School of Medicine and Barnes-Jewish Hospital in St. Louis, MO, for the use of the Siteman Flow Cytometry Core, which provided FACS services, the Washington University Siteman Cancer Center Tumor Tissue Repository. We additionally thank Amy Ly, Angela S. Archambault, Dennis Oakley, and Thomas J. Esparza for technical expertise.

References

- Bielefeldt Ohmann H, Babiuk LA. 1986. Bovine alveolar macrophages: Phenotypic and functional properties of subpopulations obtained by Percoll density gradient centrifugation. *J Leukoc Biol* 39:167–181.
- Boddeke EW, Meigel I, Frentzel S, Biber K, Renn LQ, Gebicke-Harter P. 1999. Functional expression of the fractalkine (CX3C) receptor and its regulation by lipopolysaccharide in rat microglia. *Eur J Pharmacol* 374:309–313.
- Cabanski CR, Magrini V, Griffith M, Griffith OL, McGrath S, Zhang J, Walker J, Ly A, Demeter R, Fulton RS, Pong WW, Gutmann DH, Govindan R, Mardis ER, Maher CA. 2014. cDNA hybrid capture improves transcriptome analysis on low-input and archived samples. *J Mol Diagn* 16:440–451.
- Cahoy JD, Emery B, Kaushal A, Foo LC, Zamanian JL, Christopherson KS, Xing Y, Lubischer JL, Krieg PA, Krupenko SA, Thompson WJ, Barres BA. 2008. A transcriptome database for astrocytes, neurons, and oligodendrocytes: A new resource for understanding brain development and function. *J Neurosci* 28:264–278.
- Casha S, Zygun D, McGowan MD, Bains I, Yong VW, Hurlbert RJ. 2012. Results of a phase II placebo-controlled randomized trial of minocycline in acute spinal cord injury. *Brain* 135(Pt 4):1224–1236.
- Chandler DB, Fuller WC, Jackson RM, Fulmer JD. 1986. Fractionation of rat alveolar macrophages by isopycnic centrifugation: Morphological, cytochemical, biochemical, and functional properties. *J Leukoc Biol* 39:371–383.
- Davalos D, Ryu JK, Merlini M, Baeten KM, Le Moan N, Petersen MA, Deerinck TJ, Smirnov DS, Bedard C, Hakozaki H, Gonias Murray S, Ling JB, Lassmann H, Degen JL, Ellisman MH, Akassoglou K. 2012. Fibrinogen-induced perivascular microglial clustering is required for the development of axonal damage in neuroinflammation. *Nat Commun* 3:1227.
- Davis JB, McMurray HF, Schubert D. 1992. The amyloid beta-protein of Alzheimer's disease is chemotactic for mononuclear phagocytes. *Biochem Biophys Res Commun* 189:1096–1100.
- Dheen ST, Kaur C, Ling EA. 2007. Microglial activation and its implications in the brain diseases. *Curr Med Chem* 14:1189–1197.
- Doyle JP, Dougherty JD, Heiman M, Schmidt EF, Stevens TR, Ma G, Bupp S, Shrestha P, Shah RD, Doughty ML, Gong S, Greengard P, Heintz N. 2008. Application of a translational profiling approach for the comparative analysis of CNS cell types. *Cell* 135:749–762.
- Fitzner D, Schnaars M, van Rossum D, Krishnamoorthy G, Dibaj P, Bakhti M, Regen T, Hanisch UK, Simons M. 2011. Selective transfer of exosomes from oligodendrocytes to microglia by macropinocytosis. *J Cell Sci* 124:447–458.
- Gitik M, Liraz-Zaltsman S, Oldenburg PA, Reichert F, Rotshenker S. 2011. Myelin down-regulates myelin phagocytosis by microglia and macrophages through interactions between CD47 on myelin and SIRPalpha (signal regulatory protein-alpha) on phagocytes. *J Neuroinflammation* 8:24.
- Govindan R, Ding L, Griffith M, Subramanian J, Dees ND, Kanchi KL, Maher CA, Fulton R, Fulton L, Wallis J, Chen K, Walker J, McDonald S, Bose R, Ornitz D, Xiong D, You M, Dooling DJ, Watson M, Mardis ER, Wilson RK. 2012. Genomic landscape of non-small cell lung cancer in smokers and never-smokers. *Cell* 150:1121–1134.
- Graeber MB, Scheithauer BW, Kreutzberg GW. 2002. Microglia in brain tumors. *Glia* 40:252–259.
- Hassan NF, Rifat S, Campbell DE, McCawley LJ, Douglas SD. 1991. Isolation and flow cytometric characterization of newborn mouse brain-derived microglia maintained in vitro. *J Leukoc Biol* 50:86–92.
- Heiman M, Schaefer A, Gong S, Peterson JD, Day M, Ramsey KE, Suarez-Farinas M, Schwarz C, Stephan DA, Surmeier DJ, Greengard P, Heintz N. 2008. A translational profiling approach for the molecular characterization of CNS cell types. *Cell* 135:738–748.
- Hernandez-Ontiveros DG, Tajiri N, Acosta S, Giunta B, Tan J, Borlongan CV. 2013. Microglia activation as a biomarker for traumatic brain injury. *Front Neurol* 4:30.
- Hirasawa T, Ohsawa K, Imai Y, Ondo Y, Akazawa C, Uchino S, Kohsaka S. 2005. Visualization of microglia in living tissues using Iba1-EGFP transgenic mice. *J Neurosci Res* 81:357–362.
- Hurley SD, Walter SA, Semple-Rowland SL, Streit WJ. 1999. Cytokine transcripts expressed by microglia in vitro are not expressed by amoeboid microglia of the developing rat central nervous system. *Glia* 25:304–309.
- Imai Y, Ibata I, Ito D, Ohsawa K, Kohsaka S. 1996. A novel gene Iba1 in the major histocompatibility complex class III region encoding an EF hand protein expressed in a monocytic lineage. *Biochem Biophys Res Commun* 224:855–862.
- Izzo A, Kamieniarz K, Schneider R. 2008. The histone H1 family: Specific members, specific functions? *Biol Chem* 389:333–343.
- Jack C, Ruffini F, Bar-Or A, Antel JP. 2005. Microglia and multiple sclerosis. *J Neurosci Res* 81:363–373.
- Jiang Y, Brody DL. 2012. Administration of COG1410 reduces axonal amyloid precursor protein immunoreactivity and microglial activation after controlled cortical impact in mice. *J Neurotrauma* 29:2332–2341.
- Jung S, Aliberti J, Graemmel P, Sunshine MJ, Kreutzberg GW, Sher A, Littman DR. 2000. Analysis of fractalkine receptor CX(3)CR1 function by

- targeted deletion and green fluorescent protein reporter gene insertion. *Mol Cell Biol* 20:4106–4114.
- Kaindl AM, Degos V, Peineau S, Gouadon E, Chhor V, Loron G, Le Charpentier T, Jossierand J, Ali C, Vivien D, Collingridge GL, Lombet A, Issa L, Rene F, Loeffler JP, Kavelaars A, Verney C, Mantz J, Gressens P. 2012. Activation of microglial N-methyl-D-aspartate receptors triggers inflammation and neuronal cell death in the developing and mature brain. *Ann Neurol* 72:536–549.
- Kettenmann H, Kirchhoff F, Verkhratsky A. 2013. Microglia: New roles for the synaptic stripper. *Neuron* 77:10–18.
- Khodosevich K, Inta D, Seeburg PH, Monyer H. 2007. Gene expression analysis of in vivo fluorescent cells. *PLoS One* 2:e1151.
- Klein RS. 2004. Regulation of neuroinflammation: The role of CXCL10 in lymphocyte infiltration during autoimmune encephalomyelitis. *J Cell Biochem* 92:213–222.
- Lemarchant S, Pruvost M, Montaner J, Emery E, Vivien D, Kanninen K, Koistinaho J. 2013. ADAMTS proteoglycanases in the physiological and pathological central nervous system. *J Neuroinflammation* 10:133.
- Lewis CA, Manning J, Rossi F, Krieger C. 2012. The neuroinflammatory response in ALS: The roles of microglia and T cells. *Neurol Res Int* 2012:803701.
- Liang KJ, Lee JE, Wang YD, Ma W, Fontainhas AM, Fariss RN, Wong WT. 2009. Regulation of dynamic behavior of retinal microglia by CX3CR1 signaling. *Invest Ophthalmol Vis Sci* 50:4444–4451.
- Mardis ER, Ding L, Dooling DJ, Larson DE, McLellan MD, Chen K, Koboldt DC, Fulton RS, Delehaunty KD, McGrath SD, Fulton LA, Locke DP, Magrini VJ, Abbott RM, Vickery TL, Reed JS, Robinson JS, Wylie T, Smith SM, Carmichael L, Eldred JM, Harris CC, Walker J, Peck JB, Du F, Dukes AF, Sanderson GE, Brummett AM, Clark E, McMichael JF, Meyer RJ, Schindler JK, Pohl CS, Wallis JW, Shi X, Lin L, Schmidt H, Tang Y, Haipek C, Wiechert ME, Ivy JV, Kalicki J, Elliott G, Ries RE, Payton JE, Westervelt P, Tomasson MH, Watson MA, Baty J, Heath S, Shannon WD, Nagarajan R, Link DC, Walter MJ, Graubert TA, DiPersio JF, Wilson RK, Ley TJ. 2009. Recurring mutations found by sequencing an acute myeloid leukemia genome. *N Engl J Med* 361:1058–1066.
- Matsumoto Y, Ohmori K, Fujiwara M. 1992. Microglial and astroglial reactions to inflammatory lesions of experimental autoimmune encephalomyelitis in the rat central nervous system. *J Neuroimmunol* 37:23–33.
- Meda L, Cassatella MA, Szendrei GI, Otvos L, Jr., Baron P, Villalba M, Ferrari D, Rossi F. 1995. Activation of microglial cells by beta-amyloid protein and interferon-gamma. *Nature* 374:647–650.
- Miranda KC, Bond DT, Levin JZ, Adiconis X, Sivachenko A, Russ C, Brown D, Nusbaum C, Russo LM. 2014. Massively parallel sequencing of human urinary exosome/microvesicle RNA reveals a predominance of non-coding RNA. *PLoS One* 9:e96094.
- Morimura T, Neuchrist C, Kitz K, Budka H, Scheiner O, Kraft D, Lassmann H. 1990. Monocyte subpopulations in human gliomas: Expression of Fc and complement receptors and correlation with tumor proliferation. *Acta Neuropathol* 80:287–294.
- O'Neill SJ, Hoehn SK, Lesperance E, Klass DJ. 1984. Functional heterogeneity of isopycnic fractions of rat alveolar macrophages. *Infect Immun* 46:282–284.
- Ohtaki H, Tsumuraya T, Song D, Sato A, Ohara K, Miyamoto K, Nakano H, Kiriya K, Dohi K, Hiraizumi Y, Matsunaga M, Shioda S. 2013. Establishment and characterization of primary adult microglial culture in mice. *Acta Neurochir Suppl* 118:49–54.
- Oram JF, Vaughan AM. 2000. ABCA1-mediated transport of cellular cholesterol and phospholipids to HDL apolipoproteins. *Curr Opin Lipidol* 11:253–260.
- Ozsolak F, Milos PM. 2011. RNA sequencing: Advances, challenges and opportunities. *Nat Rev Genet* 12:87–98.
- Parkhurst CN, Gan WB. 2010. Microglia dynamics and function in the CNS. *Curr Opin Neurobiol* 20:595–600.
- Penfold PL, Madigan MC, Provis JM. 1991. Antibodies to human leucocyte antigens indicate subpopulations of microglia in human retina. *Vis Neurosci* 7:383–388.
- Perry VH, Hume DA, Gordon S. 1985. Immunohistochemical localization of macrophages and microglia in the adult and developing mouse brain. *Neuroscience* 15:313–326.
- Petersohn D, Thiel G. 1996. Role of zinc-finger proteins Sp1 and zif268/egr-1 in transcriptional regulation of the human synaptobrevin II gene. *Eur J Biochem* 239:827–834.
- Plasman N, Vray B. 1993. Mouse peritoneal macrophages: Characterization of functional subsets following Percoll density gradients. *Res Immunol* 144:151–163.
- Pong WW, Higer SB, Gianino SM, Emnett RJ, Gutmann DH. 2013a. Reduced microglial CX3CR1 expression delays neurofibromatosis-1 glioma formation. *Ann Neurol* 73:303–308.
- Pong WW, Walker J, Wylie T, Magrini V, Luo J, Emnett RJ, Choi J, Cooper ML, Griffith M, Griffith OL, Rubin JB, Fuller GN, Piwnica-Worms D, Feng X, Hambarzumyan D, DiPersio JF, Mardis ER, Gutmann DH. 2013b. F11R is a novel monocyte prognostic biomarker for malignant glioma. *PLoS One* 8:e77571.
- Racke MK. 2001. Experimental autoimmune encephalomyelitis (EAE). *Curr Protoc Neurosci Chapter 9:Unit9 7*.
- Ramlackhansingh AF, Brooks DJ, Greenwood RJ, Bose SK, Turkheimer FE, Kinnunen KM, Gentleman S, Heckemann RA, Gunanayagam K, Gelosa G, Sharp DJ. 2011. Inflammation after trauma: Microglial activation and traumatic brain injury. *Ann Neurol* 70:374–383.
- Rasmussen SE, Rhodes JM, Bennedsen J, Larsen SO. 1983. Fractionation of untreated and inflammatory murine peritoneal macrophages on discontinuous Percoll density gradients. *Acta Pathol Microbiol Immunol Scand C* 91:299–304.
- Rinner WA, Bauer J, Schmidts M, Lassmann H, Hickey WF. 1995. Resident microglia and hematogenous macrophages as phagocytes in adoptively transferred experimental autoimmune encephalomyelitis: An investigation using rat radiation bone marrow chimeras. *Glia* 14:257–266.
- Roberts A, Pimentel H, Trapnell C, Pachter L. 2011a. Identification of novel transcripts in annotated genomes using RNA-Seq. *Bioinformatics* 27:2325–2329.
- Roberts A, Trapnell C, Donaghey J, Rinn JL, Pachter L. 2011b. Improving RNA-Seq expression estimates by correcting for fragment bias. *Genome Biol* 12:R22.
- Roggendorf W, Strupp S, Paulus W. 1996. Distribution and characterization of microglia/macrophages in human brain tumors. *Acta Neuropathol* 92:288–293.
- Sanz E, Yang L, Su T, Morris DR, McKnight GS, Amieux PS. 2009. Cell-type-specific isolation of ribosome-associated mRNA from complex tissues. *Proc Natl Acad Sci USA* 106:13939–13944.
- Sasaki A, Yamaguchi H, Ogawa A, Sugihara S, Nakazato Y. 1997. Microglial activation in early stages of amyloid beta protein deposition. *Acta Neuropathol* 94:316–322.
- Simmons GW, Pong WW, Emnett RJ, White CR, Gianino SM, Rodriguez FJ, Gutmann DH. 2011. Neurofibromatosis-1 heterozygosity increases microglia in a spatially and temporally restricted pattern relevant to mouse optic glioma formation and growth. *J Neuropathol Exp Neurol* 70:51–62.
- Szabo M, Gulya K. 2013. Development of the microglial phenotype in culture. *Neuroscience* 241:280–295.
- Tariq MA, Kim HJ, Jejelowo O, Pourmand N. 2011. Whole-transcriptome RNA-seq analysis from minute amount of total RNA. *Nucleic Acids Res* 39:e120.
- Tran HT, LaFerla FM, Holtzman DM, Brody DL. 2011. Controlled cortical impact traumatic brain injury in 3xTg-AD mice causes acute intra-axonal amyloid-beta accumulation and independently accelerates the development of tau abnormalities. *J Neurosci* 31:9513–9525.
- Trapnell C, Pachter L, Salzberg SL. 2009. TopHat: Discovering splice junctions with RNA-Seq. *Bioinformatics* 25:1105–1111.
- Trapnell C, Williams BA, Pertea G, Mortazavi A, Kwan G, van Baren MJ, Salzberg SL, Wold BJ, Pachter L. 2010. Transcript assembly and quantification by RNA-Seq reveals unannotated transcripts and isoform switching during cell differentiation. *Nat Biotechnol* 28:511–515.

Veillette A, Dong Z, Latour S. 2007. Consequence of the SLAM-SAP signaling pathway in innate-like and conventional lymphocytes. *Immunity* 27:698–710.

Venkatesan C, Chrzaszcz M, Choi N, Wainwright MS. 2010. Chronic upregulation of activated microglia immunoreactive for galectin-3/Mac-2 and nerve growth factor following diffuse axonal injury. *J Neuroinflammation* 7:32.

Waller R, Woodroffe MN, Francese S, Heath PR, Wharton SB, Ince PG, Sharrack B, Simpson JE. 2012. Isolation of enriched glial populations from

post-mortem human CNS material by immuno-laser capture microdissection. *J Neurosci Methods* 208:108–113.

Wang LH, Strittmatter SM. 1996. A family of rat CRMP genes is differentially expressed in the nervous system. *J Neurosci* 16:6197–6207.

Windak R, Muller J, Felley A, Akhmedov A, Wagner EF, Pedrazzini T, Sumara G, Ricci R. 2013. The AP-1 transcription factor c-Jun prevents stress-imposed maladaptive remodeling of the heart. *PLoS One* 8:e73294.